

The Rotational Dynamics of H₂ Adsorbed in Covalent Organic Frameworks

Tony Pham,^{†,§} Katherine A. Forrest,^{†,§} Matthew Mostrom,[†] Joseph R. Hunt,[‡] Hiroyasu Furukawa,[°]
Juergen Eckert,^{*,†,⊥} and Brian Space^{*,†}

[†]Department of Chemistry, University of South Florida,
4202 East Fowler Avenue, CHE205, Tampa, FL 33620-5250, United States

[‡]Center for Reticular Chemistry at the California NanoSystems Institute,
Department of Chemistry and Biochemistry, University of California–Los Angeles,
607 Charles E. Young Drive East, Los Angeles, CA 90095, United States

[°]Department of Chemistry, University of California–Berkeley,
Materials Sciences Division, Lawrence Berkeley National Laboratory,
Berkeley, CA, 94720, United States

[⊥]Department of Chemistry and Biochemistry, Texas Tech University,
2500 Broadway, Box 41061, Lubbock, TX 79409-1061, United States

[§]Authors contributed equally

*brian.b.space@gmail.com; juergen@usf.edu

Partial Charges For COF-1

The partial charges for the chemically distinct atoms in COF-1 (Figure S1) were determined through electronic structure calculations on a variety of fragments that were selected from the crystal structure of the COF. The fragments that were selected for COF-1 are shown in Figure S2. The NWChem *ab initio* simulation software¹ was used to calculate the electrostatic potential surface (ESP) for each fragment considered. The calculations were performed at the Hartree–Fock level of theory with the 6-31G* basis set applied to all atoms. The partial charges were fitted onto the atomic centers *via* the CHELPG method^{2,3} to reproduce the ESP of the fragment.

The calculated average values for each unique atom within the fragments are provided in Table S1. Note, atoms that are located on the edges of the fragment were not included in the averaging. The partial charges for all chemically distinct atoms were averaged between the fragments. The partial charges were then adjusted so that the total charge of the framework was neutral. The final tabulated results for each chemically distinct atom in COF-1 are provided in Table S2.

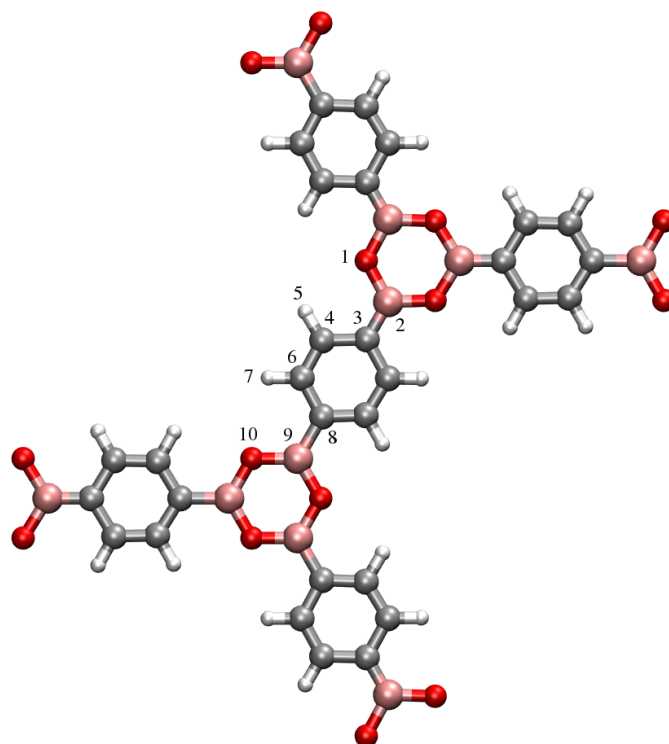


Figure S1. The numbering of the chemically distinct atoms in COF-1 as referred to in Tables S1 and S2. Atom colors: C = gray, H = white, O = red, B = pink.

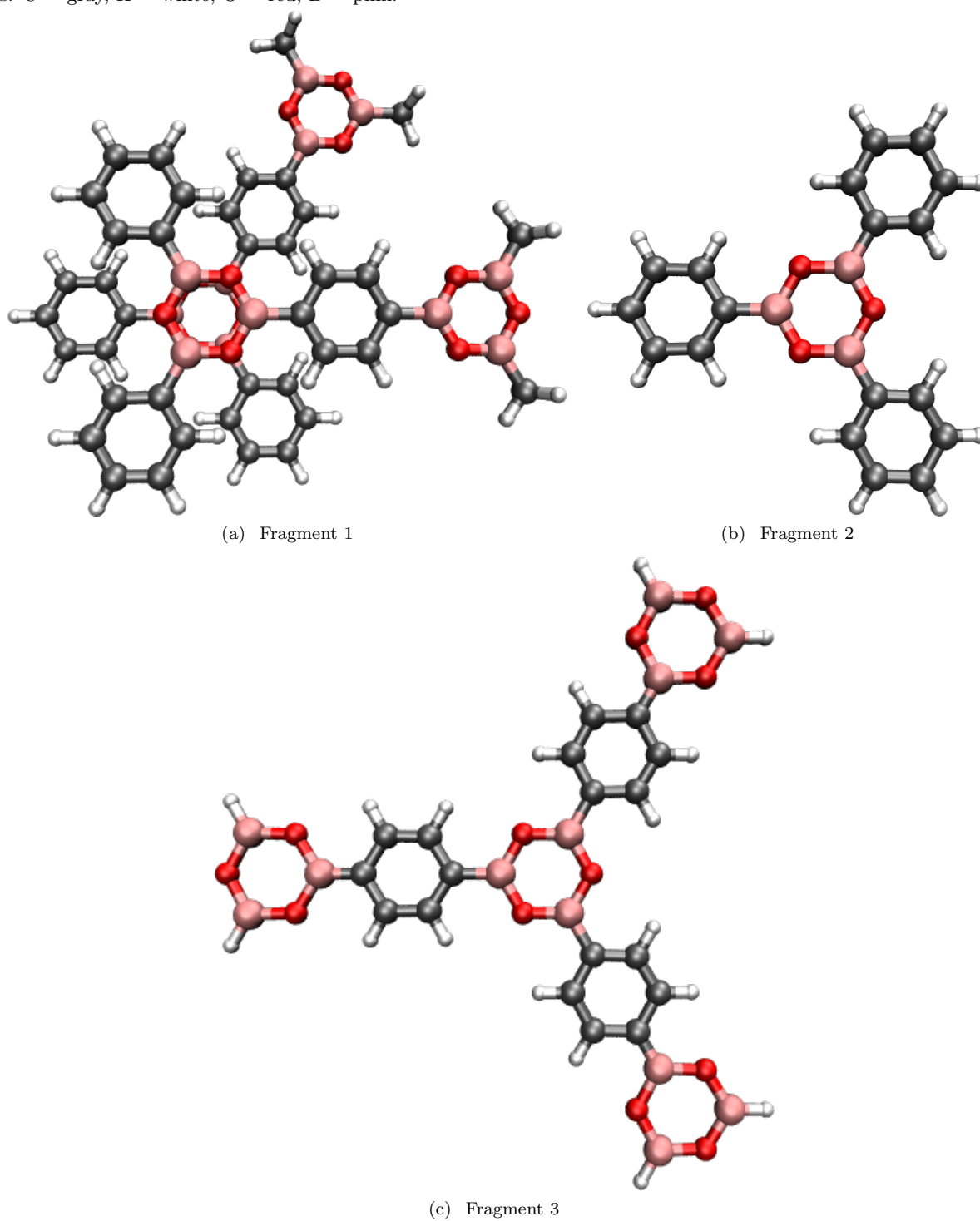
Table S1. Calculated average partial charges (e^-) for the various chemically distinct atoms for the fragments that were selected for COF-1. Labeling of atoms and fragments correspond to Figures S1 and S2, respectively.

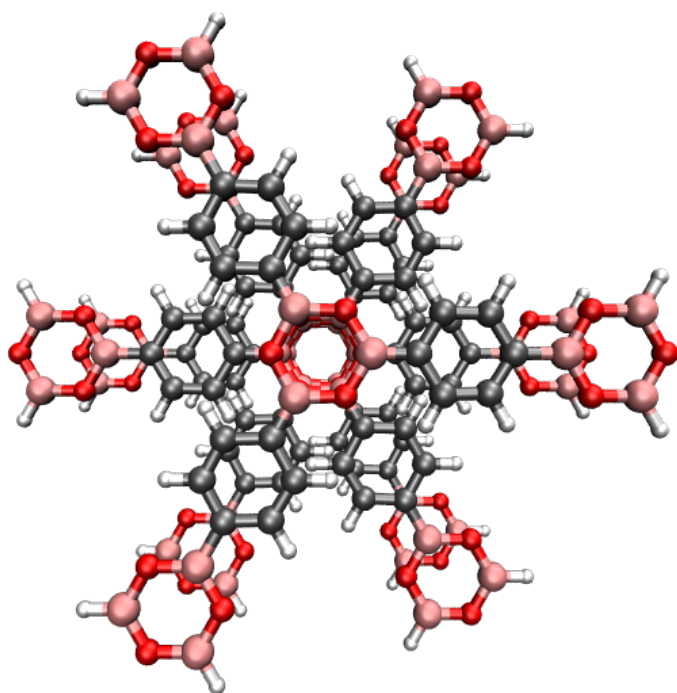
Atom	Label	Fragment 1	Fragment 2	Fragment 3	Fragment 4	Fragment 5	Fragment 6
O	1	-0.6516	-	-0.8291	-0.7151	-0.7716	-
B	2	0.8382	-	-	0.8458	0.9073	-
C	3	-0.2854	-0.0587	-0.2144	-0.2214	-0.1884	-0.2060
C	4	-0.0241	-	-0.0768	-0.0300	-0.1064	-0.0867
H	5	0.0931	-	0.1367	0.0938	-	0.1256
C	6	-0.1373	-	0.1187	-0.0779	-	-
H	7	0.1071	-	0.1135	0.1067	-	0.1029
C	8	-	-	-0.1311	-0.2298	-0.2850	-0.1869
B	9	-	0.8445	0.8391	-	-	0.8397
O	10	-	-0.6970	-0.7017	-	-	-0.6914

Table S2. The partial charges (e^-) for the chemically distinct atoms in COF-1 that were used for the simulations in COF-1 in this work. Label of atoms correspond to Figure S1.

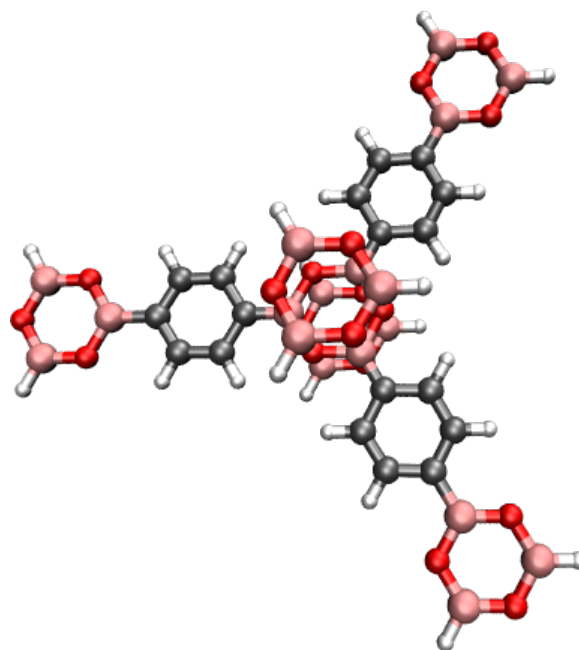
Atom	Label	$q (e^-)$
O	1	-0.72494
B	2	0.86374
C	3	-0.19125
C	4	-0.06331
H	5	0.11230
C	6	-0.10874
H	7	0.10756
C	8	-0.20345
B	9	0.84108
O	10	-0.68080

Figure S2. Fragments of COF-1 that were selected for gas phase charge fitting calculations. Label of atoms correspond to Figure S1. Atom colors: C = gray, H = white, O = red, B = pink.

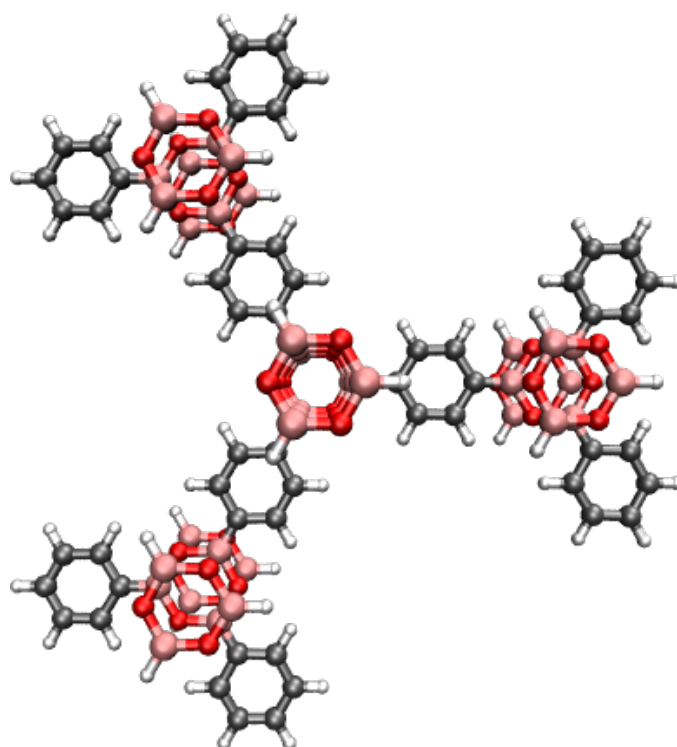




(d) Fragment 4



(e) Fragment 5



(f) Fragment 6

Partial Charges For COF-102

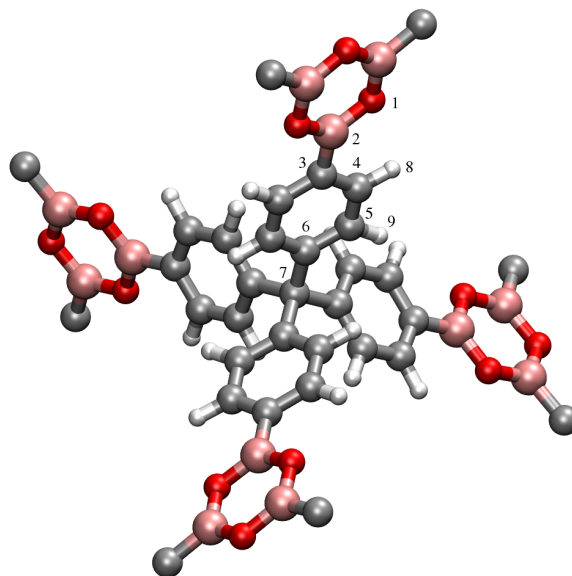


Figure S3. The numbering of the chemically distinct atoms in COF-102 as referred to in Table S3. Atom colors: C = gray, H = white, O = red, B = pink.

Table S3. The partial charges (e^-) for the chemically distinct atoms in COF-102 that were used for the simulations in COF-102 in this work. Label of atoms correspond to Figure S3. These partial charges were determined using the extended charge equilibration (EQ $_{eq}$) method.⁴

Atom	Label	q (e^-)
O	1	-1.02785
B	2	1.45683
C	3	-0.70900
C	4	0.29601
C	5	-0.24950
C	6	0.18800
C	7	-0.20800
H	8	-0.06150
H	9	0.08700

Repulsion/Dispersion Parameters

For simulations of H₂ adsorption in both COFs considered in this work, repulsion/dispersion interactions were calculated using the Lennard–Jones 12–6 potential, which is the following:⁵

$$U_{LJ} = 4\epsilon_{ij} \left[\left(\frac{\sigma_{ij}}{r_{ij}} \right)^{12} - \left(\frac{\sigma_{ij}}{r_{ij}} \right)^6 \right] \quad (1)$$

where r_{ij} is the distance between sites i and j , ϵ_{ij} is the depth of the potential well between sites i and j , and σ_{ij} is the distance between sites i and j at which $U_{LJ} = 0$. The Lennard–Jones parameters (ϵ and σ) for all C and H atoms were taken from the Optimized Potentials for Liquid Simulations – All Atom (OPLS-AA) force field,⁶ while those for O and B were taken from the Universal Force Field (UFF).⁷ The interactions between unlike species were calculated using the Lorentz–Bertholet mixing rules, which are the following:⁸

$$\epsilon_{ij} = (\epsilon_{ii}\epsilon_{jj})^{\frac{1}{2}} \quad (2)$$

$$\sigma_{ij} = \frac{1}{2}(\sigma_{ii} + \sigma_{jj}) \quad (3)$$

The repulsion/dispersion parameters that were used for the atoms in COF-1 and COF-102 for the simulations in this work are provided in Tables S4 and S5, respectively.

We note that utilizing Lennard-Jones parameters from known general purpose force fields is one of many possible choices for calculating van der Waals interactions between the COF and the H₂ molecules. In this case, the potential energy function was developed around these parameters and has been extensively tested and validated as demonstrated in the literature. Indeed, these Lennard-Jones parameters have been widely used for simulations of gas adsorption in porous materials and have been shown to produce good results in such systems.^{9–12} Nevertheless, it is actually more desirable to obtain repulsion/dispersion parameters for the COF atoms by means of electronic structure methods and such efforts are ongoing in our group.

Table S4. Lennard–Jones ϵ and σ parameters used for the various atoms in COF-1 for the simulations in this work. Label of atoms correspond to Figure S1.

Atom	Label	ϵ (K)	σ (Å)
O	1	30.19000	3.11800
B	2	90.58000	3.63800
C	3	35.25000	3.55000
C	4	35.25000	3.55000
H	5	15.11000	2.42000
C	6	35.25000	3.55000
H	7	15.11000	2.42000
C	8	35.25000	3.55000
B	9	90.58000	3.63800
O	10	30.19000	3.11800

Table S5. Lennard–Jones ϵ and σ parameters used for the various atoms in COF-102 for the simulations in this work. Label of atoms correspond to Figure S3.

Atom	Label	ϵ (K)	σ (Å)
O	1	30.19000	3.11800
B	2	90.58000	3.63800
C	3	35.25000	3.55000
C	4	35.25000	3.55000
C	5	35.25000	3.55000
C	6	35.25000	3.55000
C	7	33.23000	3.50000
H	8	15.11000	2.42000
H	9	15.11000	2.42000

Grand Canonical Monte Carlo

Simulations of H₂ adsorption in COF-1 and COF-102 were performed using grand canonical Monte Carlo (GCMC) methods.¹³ The 2 × 2 × 4 system cell and unit cell was used for COF-1 and COF-102, respectively. This method constrains the chemical potential (μ), volume (V), and temperature (T) of a simulation box containing the COF–H₂ system to be constant while allowing other thermodynamic quantities, such as the particle number (N), to fluctuate.¹³ The simulation involves randomly inserting, deleting, translating, or rotating an adsorbate molecule within the simulation box with acceptance or rejection based on a random number generator scaled by the energetic favorability of the move. For both COFs, a macroscopic crystalline environment was approximated by periodic boundary conditions with a spherical cut-off corresponding to half the shortest unit cell dimension length. All COF atoms were constrained to be rigid for the simulations. In GCMC, the average particle number, $\langle N \rangle$, was calculated by the following expression:^{14,15}

$$\langle N \rangle = \frac{1}{\Xi} \sum_{N=0}^{\infty} e^{\beta\mu N} \left\{ \prod_{i=1}^{3N} \int_{-\infty}^{\infty} dx_i \right\} N e^{-\beta U_{FH}(x_1, \dots, x_{3N})} \quad (4)$$

where Ξ is the grand canonical partition function, β is the quantity $1/kT$ (k is the Boltzmann constant), and U_{FH} is the total potential energy of the COF–H₂ system that accounts for fourth order Feynman-Hibbs quantum corrections. μ for H₂ was determined for a range of temperatures and pressures using the BACK equation of state.¹⁶ The Feynman-Hibbs corrections were applied to the total potential energy, U , for simulations at 77 and 87 K according to the following equation:¹⁷

$$U_{FH} = U + \frac{\beta\hbar^2}{24\mu_m} \left(U'' + \frac{2}{r} U' \right) + \frac{\beta^2\hbar^4}{1152\mu_m^2} \left(\frac{15}{r^3} U' + \frac{4}{r} U''' + U'''' \right) \quad (5)$$

where \hbar is the reduced Planck's constant, μ_m is the reduced mass, and the primes indicate differentiation with respect to pair separation r . For simulations at 298 K in both COFs (Figures 8 and 15), Feynman-Hibbs quantum corrections were not implemented and U was used in place of U_{FH} in equation 4.

For the simulations described in the manuscript, U was calculated by summing the repulsion/dispersion and permanent electrostatic energies. These were calculated using the Lennard–Jones 12–6 potential (equation 1) and partial charges with Ewald summation,^{18,19} respectively. Note, we also performed simulations of H₂ adsorption in both COFs with the inclusion of explicit many-body polarization; the results are presented in Figures S7 and S14. In this case, the polarization energy (as calculated using a Thole–Applequist type model)^{20–24} represents an additional term in U . Moreover, we carried out simulations of H₂ adsorption using a model that includes only Lennard–Jones parameters.²⁵ For these simulations, U was simply calculated using equation 1. Once $\langle N \rangle$ was calculated, it was converted to a value that is equivalent with the experimental quantity for H₂ uptake for each state point considered.

The excess H₂ uptake, defined as the amount of H₂ adsorbed in the pore volume of the COF in excess of the bulk gas capacity in the same free space,²⁶ was determined from a calculation that utilized an experimental pore volume (V_p) of 0.30 and 1.55 cm³ g⁻¹ for COF-1 and COF-102, respectively, and bulk gas densities (ρ_b) *via* the following expression:

$$R_{ex} = \frac{1000m(\langle N \rangle - V_p\rho_b)}{M} \quad (6)$$

where m is the molar mass of the adsorbate and M is the molar mass of the COF. The excess weight percent ($wt\%_{ex}$) of H₂ adsorbed in both COFs was calculated by:

$$wt\%_{ex} = \frac{100R_{ex}}{1000 + R_{ex}} \quad (7)$$

In GCMC, the isosteric heat of adsorption (Q_{st}) values were calculated using the following expression that is based on fluctuations in N and U :²⁷

$$Q_{st} = -\frac{\langle NU \rangle - \langle N \rangle \langle U \rangle}{\langle N^2 \rangle - \langle N \rangle^2} + kT \quad (8)$$

For all state points considered in each COF, the simulations initially consisted of 1.5×10^6 Monte Carlo steps to guarantee equilibration. The simulations continued for an additional 1.5×10^6 Monte Carlo steps to ensure reasonable ensemble averages for $\langle N \rangle$ and the Q_{st} . All simulations were performed using the Massively Parallel Monte Carlo (MPMC) code, which is currently available for download on GitHub.²⁸

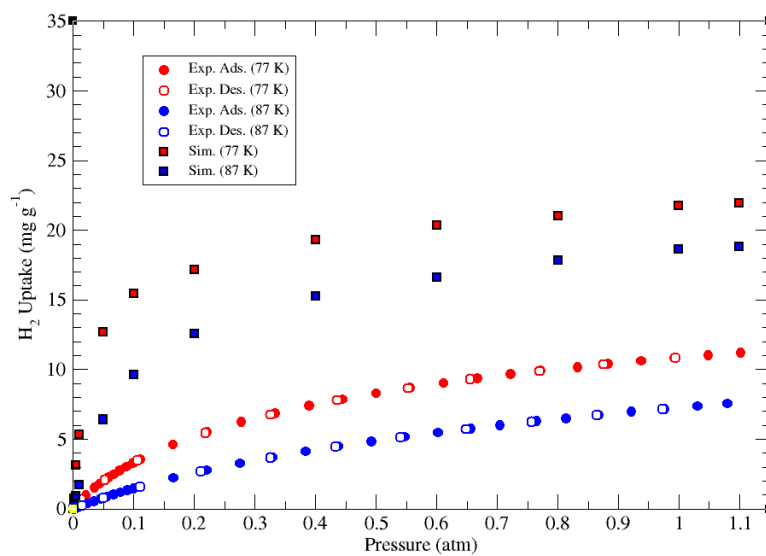
Simulated H₂ Sorption Results For COF-1

Figure S4. Low-pressure (up to 1.1 atm) absolute H₂ adsorption isotherms in COF-1 at 77 K (red) and 87 K (blue) for experiment (circles; adsorption = closed, desorption = open) and simulation (squares). The experimental data were taken from reference 29.

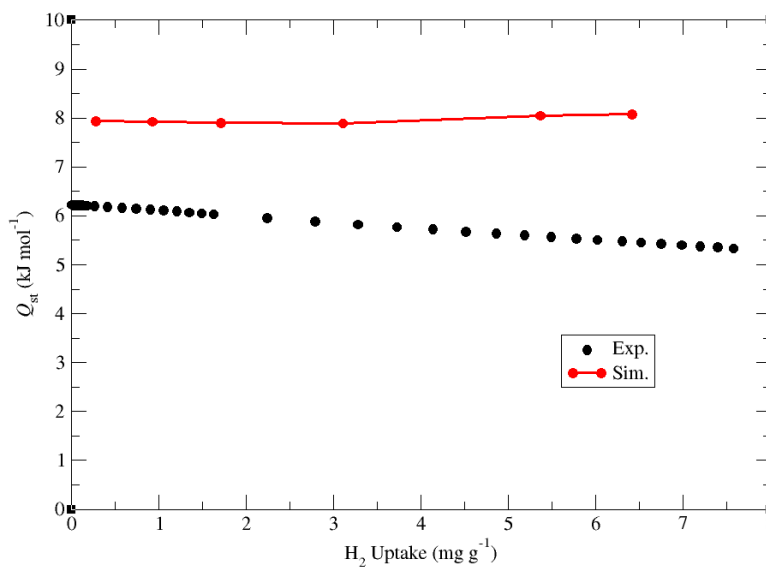


Figure S5. Isothermic heats of adsorption (Q_{st}) for H₂ in COF-1 plotted against H₂ uptakes for experiment (black) and simulation (red). The experimental data were taken from reference 29.

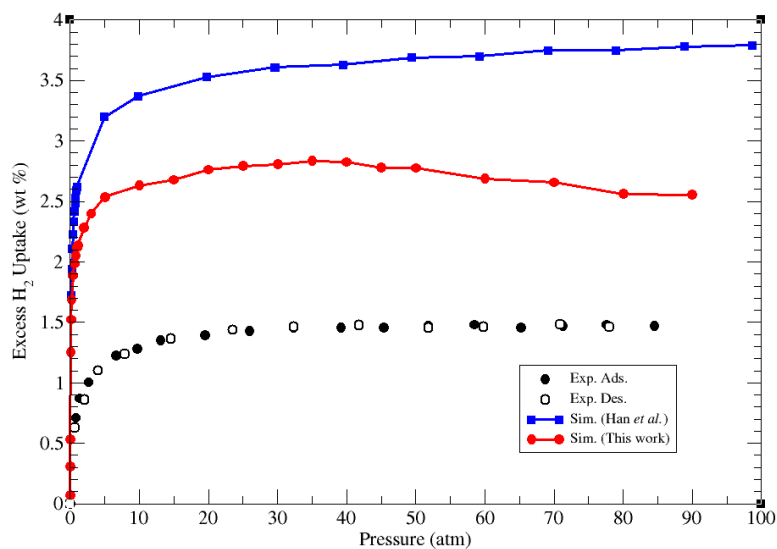


Figure S6. High-pressure (up to 90 atm) excess H₂ adsorption isotherms in COF-1 at 77 K for experiment (black circles; adsorption = closed, desorption = open) and simulations as performed by Han *et al.* (blue squares)³⁰ and those presented in this work (red circles). The experimental data were taken from reference 29.

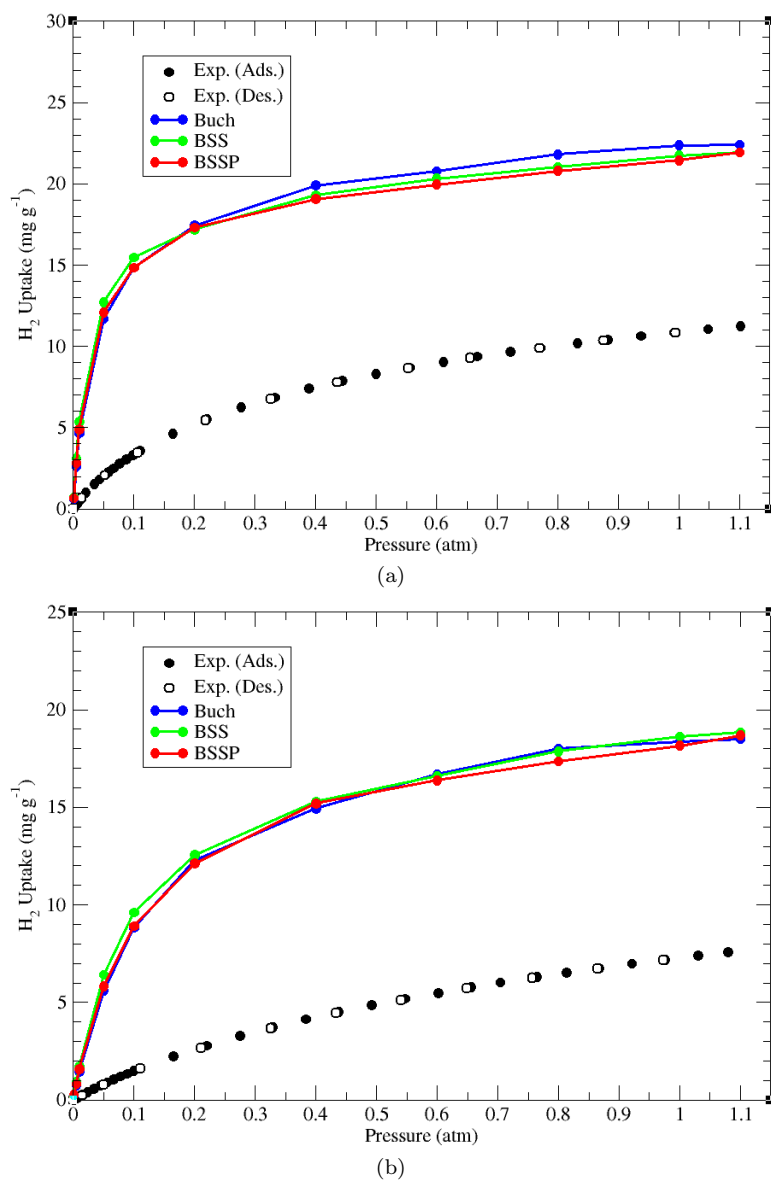


Figure S7. Low-pressure (up to 1.1 atm) absolute H₂ adsorption isotherms in COF-1 at (a) 77 K and (b) 87 K for experiment (black; adsorption = closed, desorption = open) and simulations using the Buch (blue),²⁵ BSS (green),³¹ (green),³¹ and BSSP (red) models.³¹ The experimental data were taken from reference 29. Note, the results for the BSS model are shown in Figure S4.

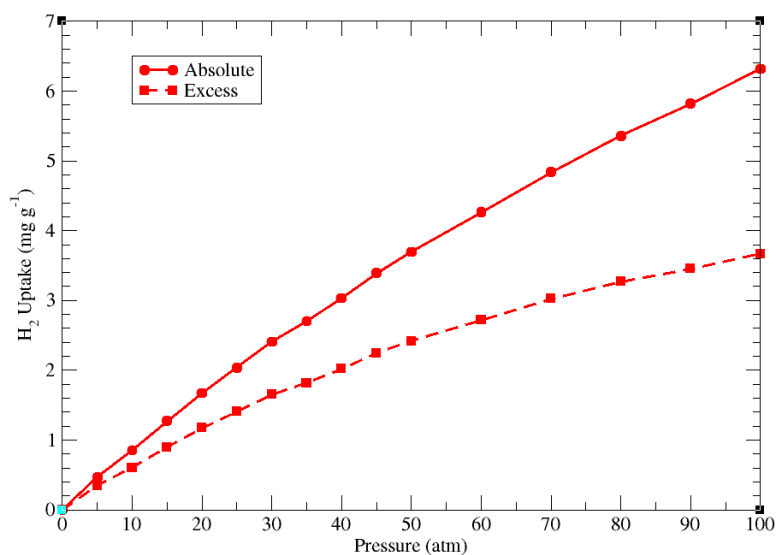


Figure S8. Simulated high-pressure (up to 100 atm) absolute (solid lines with circles) and excess (dashed lines with squares) H₂ adsorption isotherms in COF-1 at 298 K.

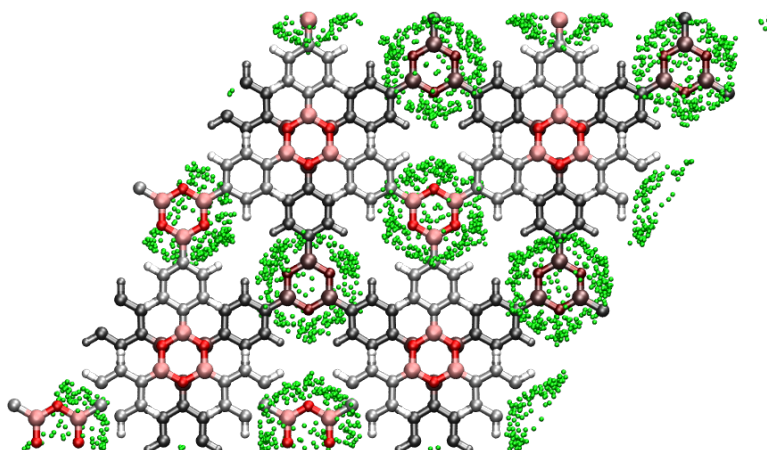


Figure S9. Orthographic *c*-axis view of the $2 \times 2 \times 4$ system cell of COF-1 showing the sites of H₂ occupancy (green). The two layers in the COF are distinguished by light and dark shading. Atom colors: C = gray, H = white, O = red, B = pink.

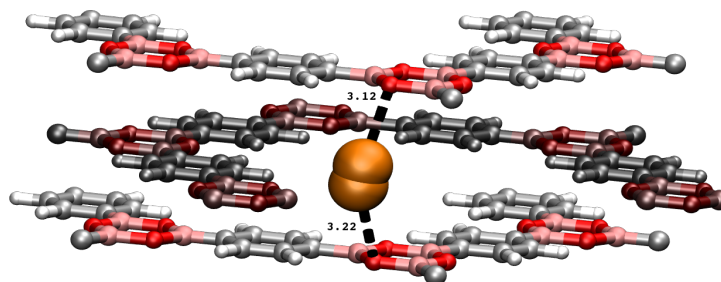


Figure S10. Molecular illustration of an adsorbed H₂ molecule between two B₃O₃ clusters of eclipsed layers in COF-1 as determined from simulated annealing calculations. The adsorbate molecule is shown in orange. The middle layer, which is staggered with respect to the top and bottom layers, is darkened for clarity. The O–H(H₂) distances are also displayed. Atom colors: C = gray, H = white, O = red, B = pink.

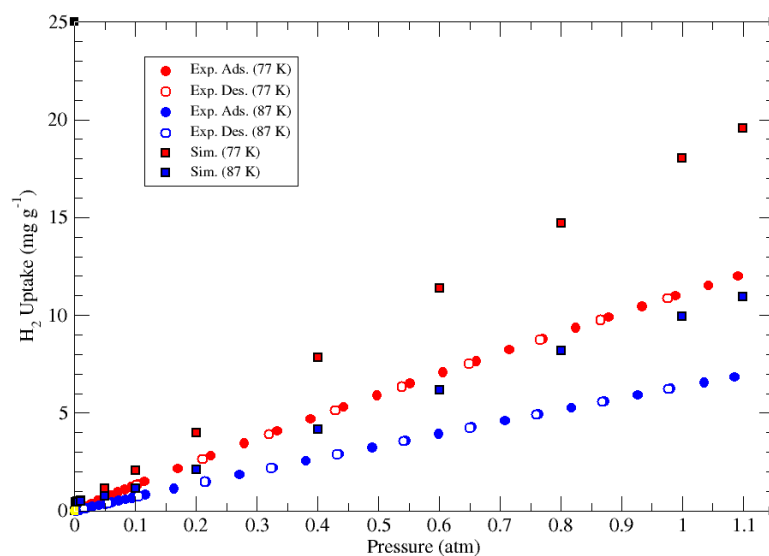
Simulated H₂ Sorption Results For COF-102

Figure S11. Low-pressure (up to 1.1 atm) absolute H₂ adsorption isotherms in COF-102 at 77 K (red) and 87 K (blue) for experiment (circles; adsorption = closed, desorption = open) and simulation (squares). The experimental data were taken from reference 29.

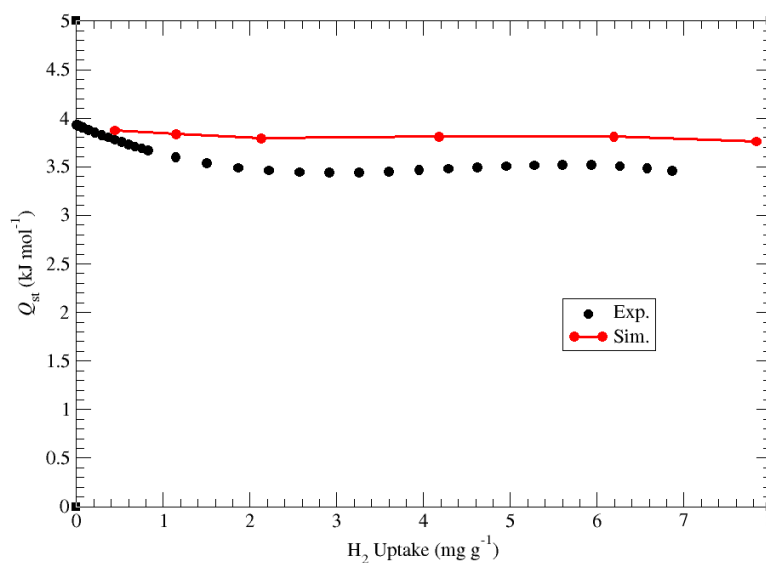


Figure S12. Isothermic heats of adsorption (Q_{st}) for H₂ in COF-102 plotted against H₂ uptakes for experiment (black) and simulation (red). The experimental data were taken from reference 29.

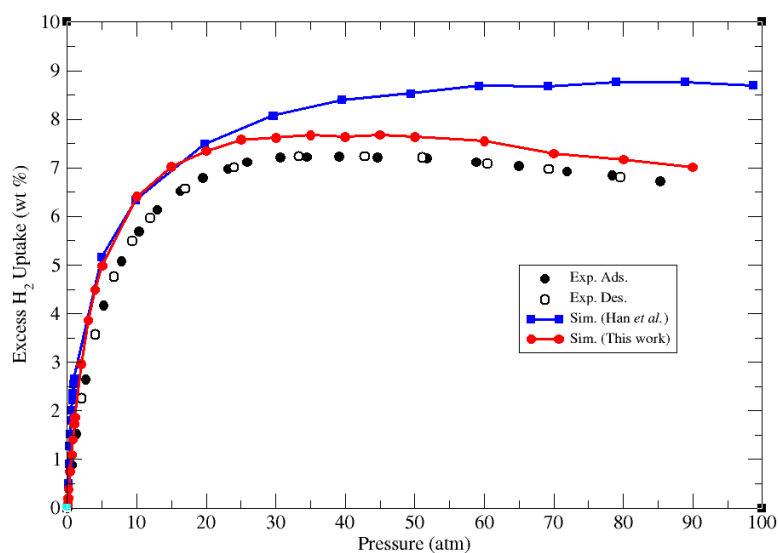


Figure S13. High-pressure (up to 90 atm) excess H₂ adsorption isotherms in COF-102 at 77 K for experiment (black circles; adsorption = closed, desorption = open) and simulations as performed by Han *et al.* (blue squares)³⁰ and those presented in this work (red circles). The experimental data were taken from reference 29.

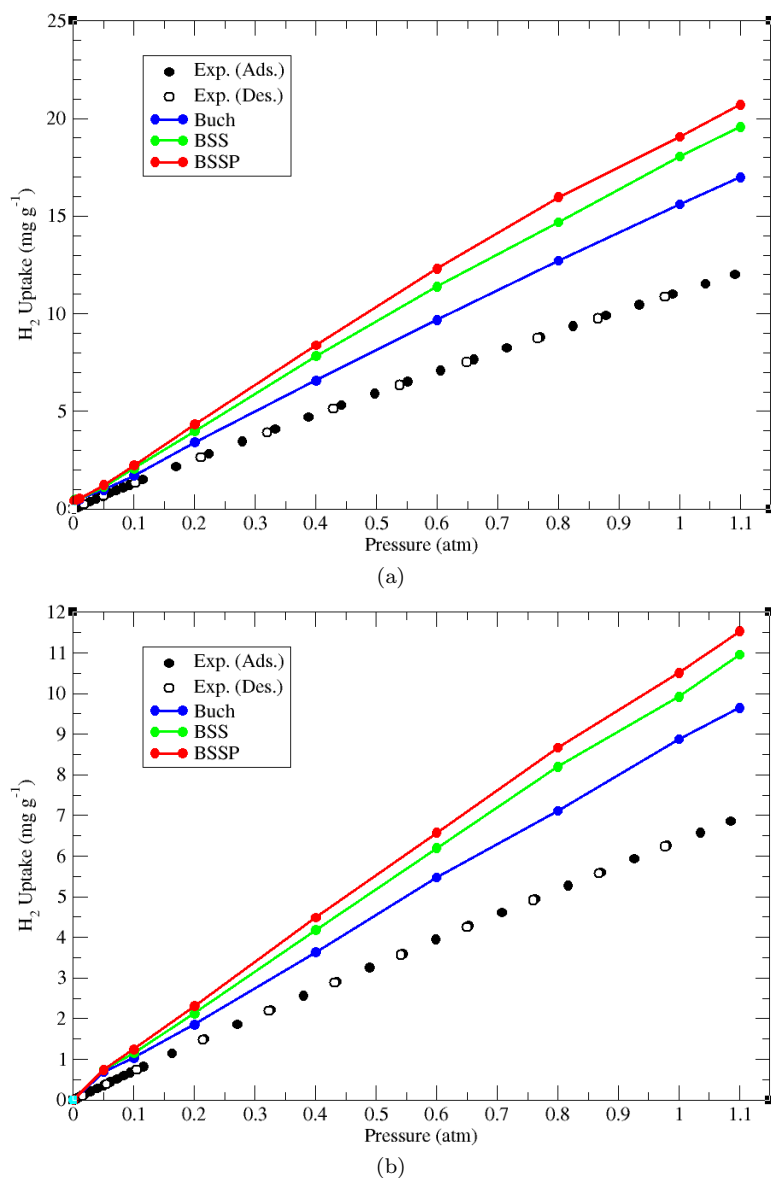


Figure S14. Low-pressure (up to 1.1 atm) absolute H₂ adsorption isotherms in COF-102 at (a) 77 K and (b) 87 K for experiment (black circles; adsorption = closed, desorption = open) and simulations using the Buch (blue),²⁵ BSS (green),³¹ (green),³¹ and BSSP (red) models.³¹ The experimental data were taken from reference 29. Note, the results for the BSS model are shown in Figure S11.

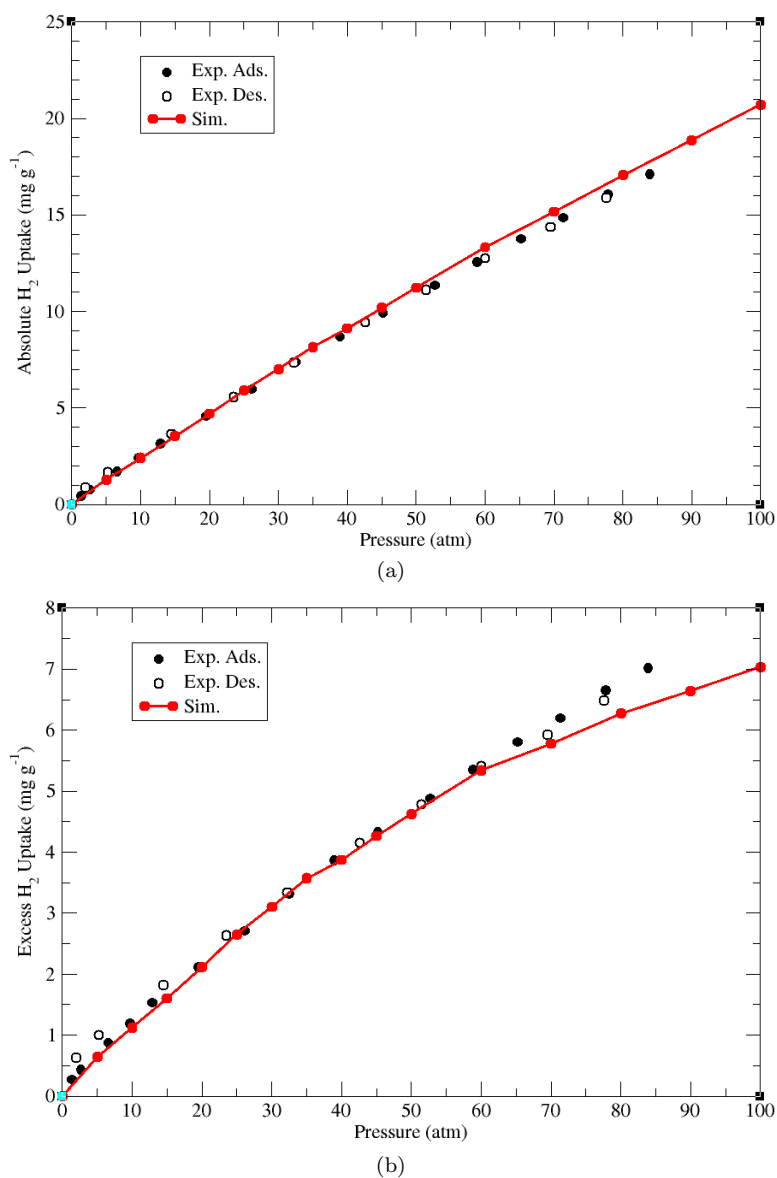


Figure S15. (a) High-pressure (up to 100 atm) absolute and (b) excess H₂ adsorption isotherms in COF-102 at 298 K for experiment (black circles; adsorption = closed, desorption = open) and simulation (red circles). The experimental data were collected on the GHP-300 gravimetric high-pressure analyzer from VTI Corporation (currently TA Instruments).²⁹

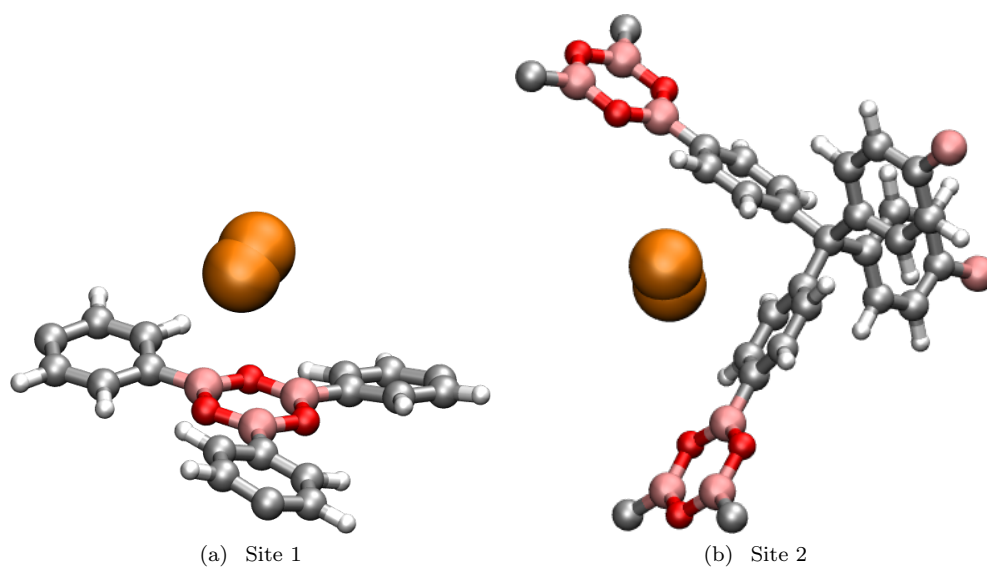


Figure S16. Molecular illustration of an adsorbed H₂ molecule about (a) site 1 and (b) site 2 in COF-102 as determined from GCMC simulations. The adsorbate molecule is shown in orange. Atom colors: C = gray, H = white, O = red, B = pink.

Quantum Rotation Calculations

The two-dimensional quantum rotational levels for a H_2 molecule adsorbed about the considered sites in COF-1 and COF-102 were calculated by diagonalizing the rotor Hamiltonian in the spherical harmonic basis, Y_{jm} , which is the following:

$$\hat{H} = B\mathbf{j}^2 + V(\theta, \phi) \quad (9)$$

where B is the rotational constant for molecular H_2 (7.35 meV),³² \mathbf{j}^2 is the angular momentum operator, and $V(\theta, \phi)$ is the potential energy surface for the rotation of the H_2 molecule with its center-of-mass held fixed within the COF- H_2 system. Each matrix element, $\langle Y_{jm} | V(\theta, \phi) | Y_{jm} \rangle$, was constructed using Gauss-Legendre quadrature³³ with a basis set consisting of $\pm m$ functions.³⁴ The potential was generated over a 16×16 quadrature grid. The kinetic energy term, $j(j+1)$, was then added to the diagonal elements. The matrix was diagonalized using the LAPACK linear algebra package,³⁵ yielding the rotational eigenvalues and the eigenvector coefficients. All two-dimensional rotational levels were calculated with $j = 7$, leading to 64 basis functions. All calculations were performed using the MPMC code.²⁸

-
- ¹ M. Valiev, E. Bylaska, N. Govind, K. Kowalski, T. Straatsma, H. V. Dam, D. Wang, J. Nieplocha, E. Apra, T. Windus and W. de Jong, *Comput. Phys. Commun.*, 2010, **181**, 1477–1489.
 - ² L. E. Chirlian and M. M. Francl, *J. Comput. Chem.*, 1987, **8**, 894–905.
 - ³ C. M. Breneman and K. B. Wiberg, *J. Comput. Chem.*, 1990, **11**, 361–373.
 - ⁴ C. E. Wilmer, K. C. Kim and R. Q. Snurr, *J. Phys. Chem. Lett.*, 2012, **3**, 2506–2511.
 - ⁵ J. Jones, *Proc. R. Soc. London, Ser. A*, 1924, **106**, 463–477.
 - ⁶ W. L. Jorgensen, D. S. Maxwell and J. Tirado-Rives, *J. Am. Chem. Soc.*, 1996, **118**, 11225–11236.
 - ⁷ A. K. Rappé, C. J. Casewit, K. S. Colwell, W. A. Goddard and W. M. Skiff, *J. Am. Chem. Soc.*, 1992, **114**, 10024–10035.
 - ⁸ M. P. Allen and D. J. Tildesley, *Computer Simulation of Liquids*, Oxford University Press, Oxford, United Kingdom, 1989.
 - ⁹ K. A. Forrest, T. Pham, K. McLaughlin, J. L. Belof, A. C. Stern, M. J. Zaworotko and B. Space, *J. Phys. Chem. C*, 2012, **116**, 15538–15549.
 - ¹⁰ Z. Zhang, Z. Li and J. Li, *Langmuir*, 2012, **28**, 12122–12133.
 - ¹¹ K. A. Forrest, T. Pham, A. Hogan, K. McLaughlin, B. Tudor, P. Nugent, S. D. Burd, A. Mullen, C. R. Cioce, L. Wojtas, M. J. Zaworotko and B. Space, *J. Phys. Chem. C*, 2013, **117**, 17687–17698.
 - ¹² S. Li, Y. G. Chung and R. Q. Snurr, *Langmuir*, 2016, **32**, 10368–10376.
 - ¹³ N. Metropolis, A. W. Rosenbluth, M. N. Rosenbluth, A. H. Teller and E. Teller, *J. Chem. Phys.*, 1953, **21**, 1087–1092.
 - ¹⁴ D. A. McQuarrie, *Statistical Mechanics*, University Science Books, Sausalito, CA, 2000.
 - ¹⁵ D. Frenkel and B. Smit, *Understanding Molecular Simulation: From Algorithms to Applications*, Academic Press, New York, 2002.
 - ¹⁶ T. Boublík, *Fluid Phase Equilib.*, 2005, **240**, 96–100.
 - ¹⁷ R. P. Feynman and A. R. Hibbs, *Quantum Mechanics and Path Integrals*, McGraw-Hill, New York, 1965.
 - ¹⁸ P. P. Ewald, *Ann. Phys.*, 1921, **369**, 253–287.
 - ¹⁹ B. A. Wells and A. L. Chaffee, *J. Chem. Theory Comput.*, 2015, **11**, 3684–3695.
 - ²⁰ J. Applequist, J. R. Carl and K.-K. Fung, *J. Am. Chem. Soc.*, 1972, **94**, 2952–2960.
 - ²¹ B. Thole, *Chem. Phys.*, 1981, **59**, 341–350.
 - ²² K. A. Bode and J. Applequist, *J. Phys. Chem.*, 1996, **100**, 17820–17824.
 - ²³ P. T. van Duijnen and M. Swart, *J. Phys. Chem. A*, 1998, **102**, 2399–2407.
 - ²⁴ K. McLaughlin, C. R. Cioce, T. Pham, J. L. Belof and B. Space, *J. Chem. Phys.*, 2013, **139**, 184112.
 - ²⁵ V. Buch, *J. Chem. Phys.*, 1994, **100**, 7610–7629.
 - ²⁶ A. L. Myers and P. A. Monson, *Langmuir*, 2002, **18**, 10261–10273.
 - ²⁷ D. Nicholson and N. G. Parsonage, *Computer Simulation and the Statistical Mechanics of Adsorption*, Academic Press, London, 1982.
 - ²⁸ J. L. Belof and B. Space, *Massively Parallel Monte Carlo (MPMC)*, Available on GitHub, 2012, <https://github.com/mpmccode/mpmc>.
 - ²⁹ H. Furukawa and O. M. Yaghi, *J. Am. Chem. Soc.*, 2009, **131**, 8875–8883.
 - ³⁰ S. S. Han, H. Furukawa, O. M. Yaghi and W. A. Goddard III, *J. Am. Chem. Soc.*, 2008, **130**, 11580–11581.
 - ³¹ J. L. Belof, A. C. Stern and B. Space, *J. Chem. Theory Comput.*, 2008, **4**, 1332–1337.
 - ³² J. Bigeleisen and M. G. Mayer, *J. Chem. Phys.*, 1947, **15**, 261–267.
 - ³³ M. Abramowitz, *Handbook of Mathematical Functions with Formulas, Graphs, and Mathematical Tables*, Dover Publications, Inc., Mineola, NY, 1965.
 - ³⁴ J. L. Belof, *Ph.D. thesis*, University of South Florida, 2009.
 - ³⁵ E. Anderson, Z. Bai, J. Dongarra, A. Greenbaum, A. McKenney, J. Du Croz, S. Hammerling, J. Demmel, C. Bischof and D. Sorensen, Proceedings of the 1990 ACM/IEEE conference on Supercomputing, 1990, pp. 2–11.